



HAL
open science

Individual heme a and heme a₃ contributions to the Soret absorption spectrum of the reduced bovine cytochrome c oxidase

Artem Diuba, Tatiana Vygodina, Natalia Azarkina, Alexander Arutyunyan, Tewfik Soulimane, Marten Vos, Alexander Konstantinov

► To cite this version:

Artem Diuba, Tatiana Vygodina, Natalia Azarkina, Alexander Arutyunyan, Tewfik Soulimane, et al.. Individual heme a and heme a₃ contributions to the Soret absorption spectrum of the reduced bovine cytochrome c oxidase. *Biochimica biophysica acta (BBA) - Bioenergetics*, 2023, 1864, pp.148937. <10.1016/j.bbabbio.2022.148937>. <hal-03862370>

HAL Id: hal-03862370

<https://hal.science/hal-03862370v1>

Submitted on 2 Nov 2023

HAL is a multi-disciplinary open access archive for the deposit and dissemination of scientific research documents, whether they are published or not. The documents may come from teaching and research institutions in France or abroad, or from public or private research centers.

L'archive ouverte pluridisciplinaire **HAL**, est destinée au dépôt et à la diffusion de documents scientifiques de niveau recherche, publiés ou non, émanant des établissements d'enseignement et de recherche français ou étrangers, des laboratoires publics ou privés.



HAL Authorization

1 Individual heme *a* and heme *a*₃ contributions to the Soret
2 absorption spectrum of the reduced bovine cytochrome *c* oxidase

3 Artem V. Diuba^{a1*}, Tatiana V. Vygodina^b, Natalia V. Azarkina^c, Alexander M.
4 Arutyunyan^d, Tewfik Soulimane^e, Marten H. Vos^f, Alexander A. Konstantinov^{g†}

5
6 ^a Belozersky Institute of Physico-Chemical Biology, Lomonosov Moscow State
7 University, Leninskie Gory 1, Bld.40, Moscow, Russia 119992 dyubon@gmail.com

8 ^b Belozersky Institute of Physico-Chemical Biology, Lomonosov Moscow State
9 University, Leninskie Gory 1, Bld.40, Moscow, Russia 119992 vygodina@belozersky.msu.ru

10 ^c Belozersky Institute of Physico-Chemical Biology, Lomonosov Moscow State
11 University, Leninskie Gory 1, Bld.40, Moscow, Russia 119992 azarkina@yahoo.com

12 ^d Belozersky Institute of Physico-Chemical Biology, Lomonosov Moscow State
13 University, Leninskie Gory 1, Bld.40, Moscow, Russia 119992 alarut@genebee.msu.ru

14 ^e Materials and Surface Science Institute, University of Limerick, Ireland V94 T9PX
15 Tewfik.Soulimane@ul.ie

16 ^f LOB, CNRS, INSERM, Ecole Polytechnique, Institut Polytechnique de Paris, Palaiseau,
17 France 91128 marten.vos@polytechnique.edu

18 ^g Belozersky Institute of Physico-Chemical Biology, Lomonosov Moscow State
19 University, Leninskie Gory 1, Bld.40, Moscow, Russia 119992

20 *Corresponding author; e-mail: dyubon@gmail.com

21 ¹Present address: Institute for Neurosciences of Montpellier, University of Montpellier,
22 Institut National de la Santé et de la Recherche Médicale, 34091 Montpellier, France

23 [†]Deceased, May 1, 2020

24
25 **CRedit author statement**

26 **Artem V. Diuba:** Conceptualization, Methodology, Software, Validation, Formal
27 analysis, Investigation, Resources, Data Curation, Writing - Original Draft, Writing - Review &
28 Editing, Visualization, Project administration. **Tatiana V. Vygodina:** Methodology, Validation,
29 Investigation, Resources, Writing - Review & Editing. **Natalia V. Azarkina:** Methodology,
30 Validation, Investigation, Resources, Writing - Review & Editing. **Alexander M. Arutyunyan:**
31 Methodology, Resources, Validation, Writing - Review & Editing. **Tewfik Soulimane:**
32 Validation, Resources, Writing - Review & Editing. **Marten H. Vos:** Conceptualization,

33 Methodology, Validation, Formal analysis, Investigation, Resources, Data Curation, Writing -
34 Review & Editing. **Alexander A. Konstantinov**: Conceptualization, Methodology, Validation,
35 Writing - Original Draft, Writing - Review & Editing, Supervision, Project administration,
36 Funding acquisition.

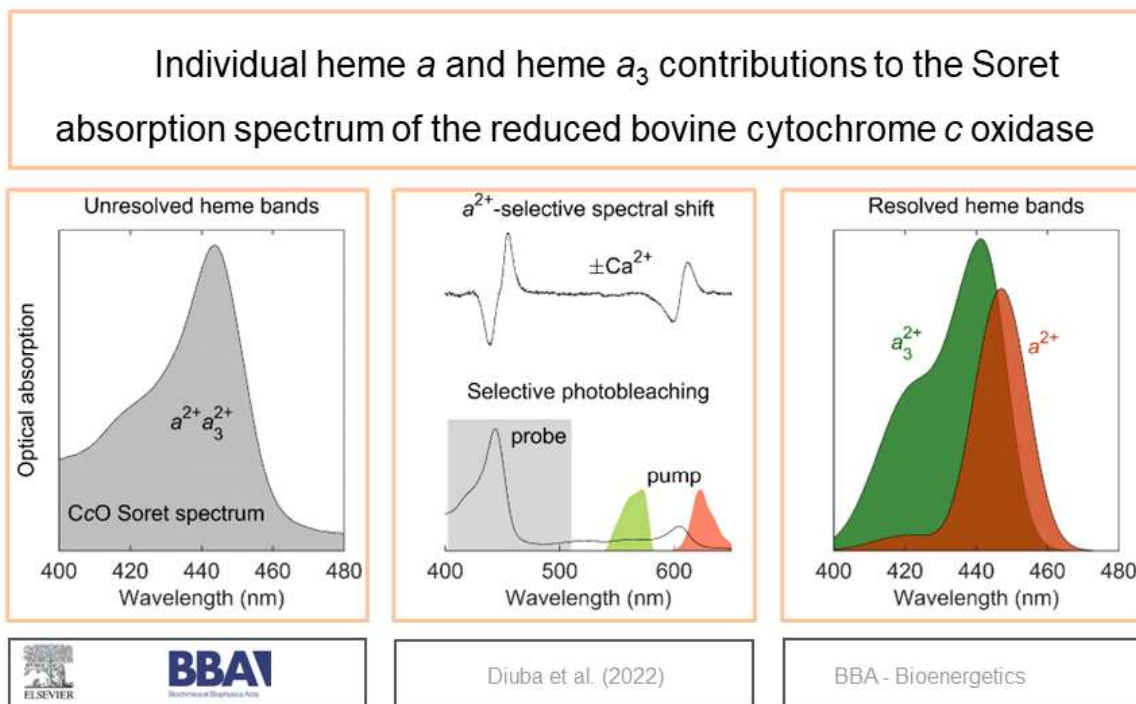
37

38 The authors declare that they have no known competing financial interests or personal
39 relationships that could have appeared to influence the work reported in this paper.

40

41

Graphical abstract:



45 **Abstract**

46 Bovine cytochrome *c* oxidase (CcO) contains two hemes, *a* and *a*₃, chemically identical
47 but differing in coordination and spin state. The Soret absorption band of reduced *aa*₃-type
48 cytochrome *c* oxidase consists of overlapping bands of the hemes *a*²⁺ and *a*₃²⁺. It shows a
49 peak at ~444 nm and a distinct shoulder at ~425 nm. However, attribution of individual
50 spectral lineshapes to hemes *a*²⁺ and *a*₃²⁺ in the Soret is controversial. In the present work,
51 we characterized spectral contributions of hemes *a*²⁺ and *a*₃²⁺ using two approaches. First, we
52 reconstructed bovine CcO heme *a*²⁺ spectrum using a selective Ca²⁺-induced spectral shift of
53 the heme *a*²⁺. Second, we investigated photobleaching of the reduced *Thermus thermophilus*
54 *ba*₃- and bovine *aa*₃-oxidases in the Soret induced by femtosecond laser pulses in the Q-
55 band. The resolved spectra show splitting of the electronic B_{0x} -, B_{0y}-transitions of both
56 reduced hemes. The heme *a*²⁺ spectrum is shifted to the red relative to heme *a*₃²⁺ spectrum.
57 The ~425 nm shoulder is mostly attributed to heme *a*₃²⁺.

58
59 **Keywords:** Cytochrome *c* oxidase, absorption spectra, femtosecond pump-probe
60 spectroscopy.

61 **Abbreviations:**

62 CcO, cytochrome *c* oxidase

63 FWHH, full width at half-height

64 MCD, magnetic circular dichroism

65 SMR, succinate: menaquinone reductase

66 **Highlights:**

- 67 • Bovine CcO *a*²⁺ Soret band is a split electronic 447.5-nm peak with a minimal
68 short-wavelength satellite
- 69 • *a*²⁺ α-band is also split
- 70 • *a*₃²⁺ Soret band is a split electronic 441-nm peak with a short-wavelength satellite
- 71 • Ratio of integrals under *a*²⁺ and *a*₃²⁺ Soret bands is approximately 1 to 2
- 72
- 73
- 74

75 1. Introduction

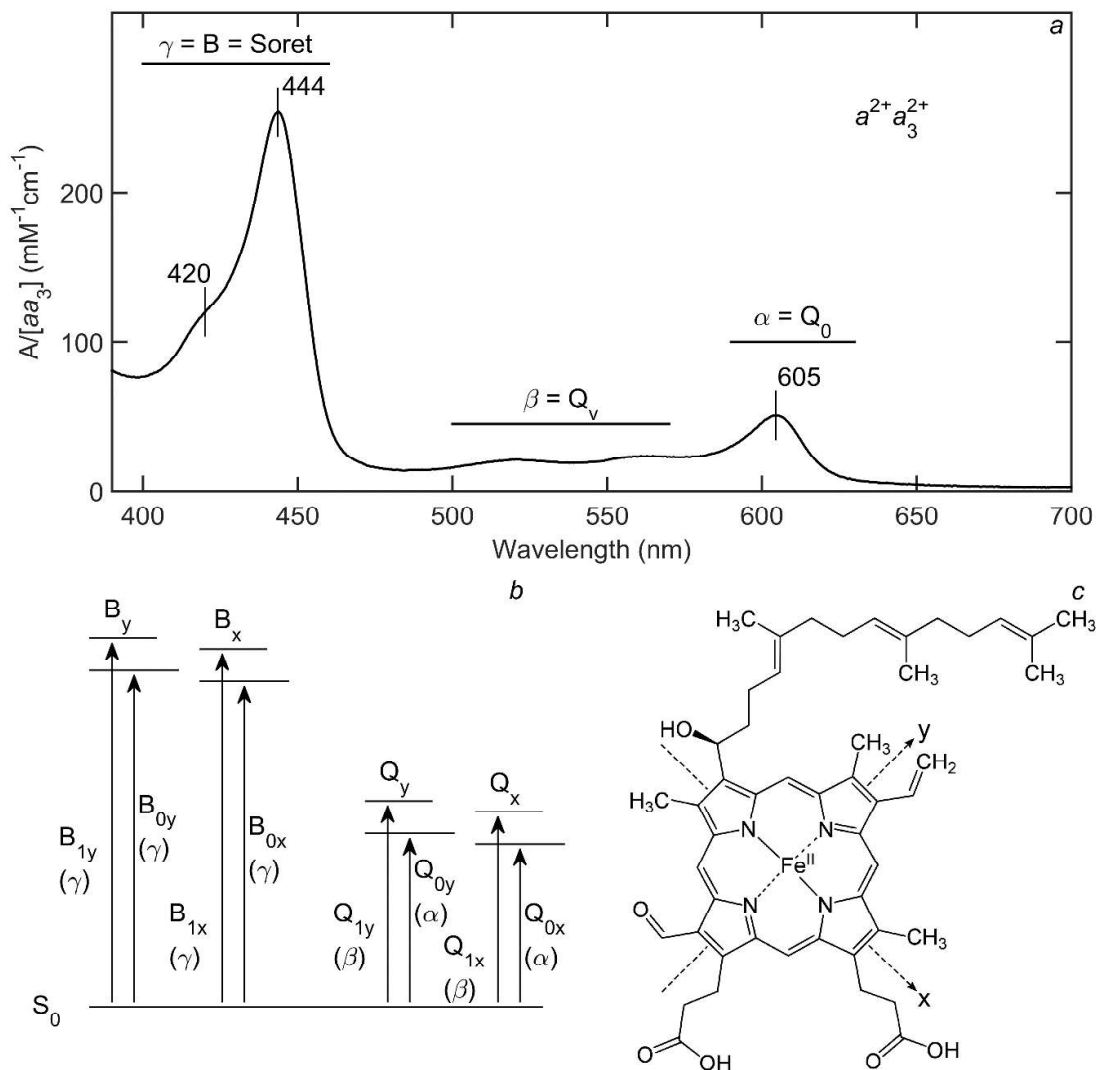
76 In mitochondrial and some bacterial respiratory chains, aa_3 -type cytochrome *c* oxidase
77 (CcO) catalyzes oxidation of ferrous cytochrome *c* by oxygen, converting redox potential
78 energy to the transmembrane difference of proton electrochemical potentials, $\Delta\mu\text{H}^+$. The
79 exergonic electron transfer coupled to proton translocation across the membrane [1] via
80 proton channels [2–6] is mediated by two A-type hemes, low-spin 6-coordinate *a* and high-
81 spin 5-coordinate a_3 , and two copper centers: binuclear Cu_A and mononuclear Cu_B [5,7–9].

82 Absorption spectra of hemes *a* and a_3 , sensitive to their redox and spin state, are
83 routinely used to monitor the reaction. **Fig. 1** shows the absorption spectrum of dithionite-
84 reduced bovine CcO. The heme absorption spectra (350-700 nm, **Fig. 1a**) display empirically
85 defined α -, β - and γ - (Soret) bands corresponding to the electronic and vibronic transitions
86 from the same ground state to increasingly higher-energy excited states (**Fig. 1b**). Platt's
87 convention [10] denotes the Soret band as B-band and groups the α - and β -bands into the Q-
88 ("visible") band. The α - and γ -bands comprise two perpendicular electronic transitions each
89 (Q_{0x} , Q_{0y} and B_{0x} , B_{0y} , respectively) oriented in the porphyrin plane (**Fig. 1c**). Each of the four
90 purely electronic transitions may have a vibronic satellite due to transition to a non-zero
91 vibrational state (for example, B_{1y} , etc). The β -band comprises vibronic satellites of the α -
92 band.

93 While heme *a* absorption dominates the Q-band, overlapping heme *a* and a_3 bands with
94 high and similar intensities challenge spectral interpretation in the Soret. The Soret band of
95 reduced bovine CcO shows a main peak at 443-444 nm accompanied by a shoulder at ~425
96 nm (**Fig. 1a**). Our current knowledge of individual absolute spectra of hemes a^{2+} and a_3^{2+}
97 relies on Vanneste's indirect derivation [11] based on variable-valence vs unliganded state
98 spectral comparison referenced to the action spectrum of CO photodissociation from yeast
99 CcO as the absolute spectrum of CO-bound heme a_3^{2+} . A 444-nm peak/~428-nm shoulder
100 pair and a symmetric 442.5-nm peak (with a weak shoulder at ~420 nm) are therein
101 respectively attributed to heme a^{2+} and heme a_3^{2+} (Fig. 5 in ref. [11] and **Fig. A.1**); these
102 spectra are included in the textbooks and monographs (e.g. [12]). However, bovine CcO
103 reduction kinetics analysis led Orii [13] to essentially opposite assignment of a featureless
104 ~445-nm peak and the asymmetric band with a short-wavelength shoulder at ~428 nm to
105 hemes a^{2+} and a_3^{2+} , respectively (see **Fig. A.1**).

106 In this work, we resolve individual absolute absorption spectra of the reduced bovine
107 CcO hemes *a* and a_3 using two yet different approaches. First, we reconstructed the heme a^{2+}

108 spectrum from Ca^{2+} -induced spectral shift. Second, we selectively excited hemes a^{2+} and a_3^{2+}
 109 with femtosecond laser pulses and measured photobleaching spectra of the two hemes. Both
 110 approaches showed B_{0x}/B_{0y} -splitting in both hemes, heme a^{2+} transitions red-shifted relative
 111 to heme a_3^{2+} transitions, and the ~ 425 nm shoulder attributed mostly to heme a_3^{2+} spectrum.
 112



113 **Fig. 1. Absorption bands of reduced cytochrome c oxidase.** (a) experimental
 114 absorption spectrum of “activated” (see 2.1) CcO (1.7 μM) bovine CcO reduced by dithionite.
 115 (b) electronic (Q_{0x} , Q_{0y} and B_{0x} , B_{0y}) and first vibronic (Q_{1x} , Q_{1y} and B_{1x} , B_{1y}) transitions from
 116 the ground state S_0 corresponding to the α -, β - and γ - absorption bands for single hemes. (c)
 117 orientation of the x,y-transitions in the plane of porphyrin ring of heme A.
 118

119 **2. Materials and methods**

120 *2.1. Reagents and preparations.* *aa*₃-type CcO was isolated from bovine heart
121 mitochondria according to [14] modified as described in [15] and dissolved in 25-50 mM
122 HEPES containing 0.05% DM. The concentration of the enzyme was determined from
123 “dithionite-reduced *minus* oxidized” difference absorption spectra using an extinction
124 coefficient $\Delta\epsilon_{605-630}$ of 27 mM⁻¹cm⁻¹. Before KCN binding, CcO was “activated” as follows.
125 Argon-deoxygenized ~30 μ M CcO in 100mM HEPES/tris pH 8.0 was reduced by a small
126 amount of dithionite in the presence of 20 μ M of hexaammineruthenium (Ru(NH₃)₆³⁺; RuAm)
127 for 30 minutes until full reduction. Dithionite and RuAm were subsequently removed using
128 centrifugal filter devices (Amicon Ultra-4, Millipore). *ba*₃-type CcO purified from *Thermus*
129 *thermophilus* was prepared as described [16]. The concentration of the *ba*₃ CcO was
130 determined using extinction coefficient $\Delta\epsilon_{560-590} = 26$ mM⁻¹cm⁻¹ for the absolute spectrum of
131 the fully reduced oxidase [17]. Succinate-menaquinone reductase preparation was a
132 generous gift from Prof. Lars Hederstedt (Lund University, Sweden). The concentration of the
133 enzyme was determined from “dithionite-reduced *minus* oxidized” difference absorption
134 spectra using an extinction coefficient $\Delta\epsilon_{558-575}$ of 45 mM⁻¹cm⁻¹ [18].

135 *2.2. Static spectroscopy.* Absorption spectra were recorded in a Cary-300 Bio
136 spectrophotometer in 1 ml quartz semi-micro cuvettes with a 1 cm optical path. A magnetic
137 circular dichroism spectrum was recorded at room temperature in a quartz cuvette with a
138 custom-built dichrograph (effective magnetic field ~ 0.7T for a 1 cm cell). The difference
139 between direct and reverse magnetic field spectra was calculated to eliminate the contribution
140 of the natural circular dichroism.

141 *2.3. Femtosecond selective photobleaching of the hemes.* Multicolor pump-probe
142 spectroscopy was performed with a setup based on a Quantronix Integra-C Ti-Saph oscillator/
143 amplifier system, delivering ~100 fs, 1.0 mJ pulses centered at 780 nm and operated at a
144 repetition rate of 500 Hz. Pump pulses with different spectral characteristics (maxima at 623,
145 608, and 570 nm for the experiments with *aa*₃; 623 and 570 nm for the experiments with *ba*₃)
146 with an energy of ~1 μ J were generated using a home-built, BBO-based (1 mm thick, $\theta=29.2^\circ$)
147 type I non-collinear optical amplifier (NOPA [19]). The NOPA was pumped with pulses
148 centered at 390 nm, generated by second harmonic generation of part of the 780-nm
149 fundamental beam in a 1-mm $\theta=32^\circ$ BBO crystal, and seeded with white light continuum
150 generated by focusing part of the 780-nm beam on a 1 mm sapphire plate; the continuum was
151 subsequently filtered appropriately using selected sharp edge interference filters (Semrock).

152 White light probe pulses were generated by focusing part of the fundamental on a 1 mm-thick
153 CaF₂ window that was continuously translated perpendicular to the beam. The probe beam
154 was dispersion-minimized around 435 nm by passing through a prism compressor, and then
155 separated into the test and reference beams. After passing through the sample, the beams
156 were dispersed and detected, shot-by-shot, on a CCD camera (Roper Scientific, SPEC-10)
157 configured as a dual-array detector.

158 To mimic isotropic conditions, the polarization of the pump beam was set at 54.7°
159 («magic angle») relative to polarization of the probe beam using a polarizer and a half-wave
160 plate. To vary delay between the pump and probe pulses, the pump beam was passed
161 through a delay line comprised of a retroreflector mounted on a step-motor driven translation
162 stage. The 1-mm optical pathlength sample cell was rastered in a Lissajous scanner to
163 ensure optimal exchange of the sample in the interaction volume. For every type of pump
164 pulse, 10 spectrokinetics sets were recorded in the range 400-500 nm (spectral resolution ~1
165 nm) and with temporal steps of 83 fs from -1 to 2 ps and of 2 ps from 2 to 50 ps. Due to
166 dispersion the effective zero time depended on the wavelength, varying the onset of the
167 absorption changes for up to 700 fs. We accounted for this dispersion during data processing.

168 *2.4. Preparation of the samples for the femtosecond spectroscopy.* Enzymes were
169 diluted in 200 mM HEPES/Tris buffer, pH ~ 7, with 0.05% DM dodecylmaltoside and 0.5 mM
170 Na-EDTA. Quartz cuvettes with a 1 mm optical pathway (“Hellma-Analytics”), type 110-QS
171 were filled with the sample and hermetically closed with plug-type rubber sleeve stoppers
172 (“Kimble”, USA). CcO and succinate: menaquinone reductase (SMR) were reduced with a
173 fresh 0.2M sodium dithionite solution (final concentration ca. 1-5 mM dithionite). To prepare
174 the dithionite solution, degassed MilliQ was added to degassed dithionite powder into an
175 argon-filled vial. The sample in the cuvette was degassed with a vacuum pump and the
176 volume above the sample was saturated with argon. Dithionite was added through the
177 stopper using a Hamilton syringe, and the volume above the sample was again saturated with
178 argon. Reduction was considered complete if the absorption spectrum corresponded to the
179 reduced form (in the case of CcO showing maxima at 444 nm and 605 nm) and stayed
180 unchanged for at least 10 minutes. The absorption in the Soret band of the reduced form was
181 0.8-1.0 OD.

182 *2.5. Data analysis.* Global analysis of the pump-induced absorption changes was
183 performed using Glotaran software [20] to extract the fastest evolution-associated spectra
184 (EASs) with correction for the instrumental response function, zero-time dispersion and

185 coherent artifacts. Prior to global analysis, noise in the data was reduced using singular value
186 decomposition. Relaxation included typically three phases with characteristic times of ca. 0.2,
187 1 and 5 ps, the fastest component representing photobleaching. Additional components did
188 not improve the fit. Decompositions into gaussians were performed in MATLAB using the
189 'Interior-point' algorithm [21–23] to minimize the mean square difference between the
190 experimental and simulated curves.

191

192

193 3. Results

194 3.1. *Reconstruction of heme a^{2+} absorption bands using Ca^{2+} -induced spectral shift.* In
195 CcO from vertebrate mitochondria, a specific cation-binding site in subunit I near heme *a* and
196 Cu_A reversibly binds Ca^{2+} and Na^+ ions [24–26]. Ca^{2+} red-shifts the entire heme *a* absorption
197 spectrum by ~ 1 nm [24,27]. The shift is small compared to the linewidths of the heme a^{2+}
198 absorption bands, so the difference spectrum of the shift represents the differential of the
199 absolute a_3 -free heme a^{2+} spectrum, and can be used to derive the heme a^{2+} absolute
200 spectrum lineshape [28].

201 We first compared the Ca^{2+} -induced spectral shift in the fully reduced unliganded
202 complex $a^{2+}a_3^{2+}$ and the mixed-valence cyanide complex $a^{2+}a_3^{3+}$ -CN (**Fig. 2a,b**). In contrast to
203 absolute spectra (**Fig. 2a**), the Ca^{2+} -induced difference spectra (**Fig. 2b**) for these two states
204 are virtually identical both in the Soret and the visible. This finding confirms that heme a^{2+} is a
205 unique contributor to the Ca^{2+} -induced spectral changes. Thus, the non-zero a_3^{2+} contribution
206 put forward earlier [24] is not supported by our data obtained using a more stable reduction
207 system. It also shows that the heme *a* spectrum is not affected by the redox and spin state of
208 heme a_3 .

209 We chose the $a^{2+}a_3^{3+}$ -CN complex as the starting point to better separate the
210 overlapping γ -peaks and minimize any possible interference from heme a_3 . The absolute
211 $a^{2+}a_3^{3+}$ -CN spectrum (**Fig. 2a**, black) showed a split Soret band with maxima at 442 nm and
212 430 nm (mainly heme a^{2+} and heme a_3^{3+} -CN, respectively) and rather symmetric α -band at
213 605 nm.

214 The corresponding difference spectrum (**Fig. 2b**, black) is dominated by narrow 1st –
215 derivative-like features in the Soret and in the visible. The Soret band signal shows A_{\min} at
216 438 nm, A_{\max} at 460 nm and a zero-crossing point at 449 nm, that coincides with neither of
217 the two maxima in the parent absolute spectrum. An inflection around the zero-crossing point

218 suggests juxtaposition of two overlapping 1st derivative-shaped components [24,28]. In the
219 visible, the difference spectrum shows the zero-crossing point at 605 nm, close to the
220 maximum of heme a^{2+} . A small derivative-shaped feature centered around 520 nm may
221 correspond to a red shift of the β -band of heme a^{2+} .

222 The integral of this differential spectrum in **Fig. 2b** gives the reconstructed lineshape of
223 the heme a^{2+} absolute spectrum (**Fig. 2c**, black). A weak baseline (**Fig. 2b**, green dotted line)
224 was subtracted from the difference spectrum before integration to avoid negative values in the
225 reconstructed spectrum. We decomposed the spectral lineshape into a sum of gaussians with
226 the following assumptions:

227 (1) the Soret and α -band are comprised of two individual electronic transitions (cf. **Fig.**
228 **1b,c**);

229 (2) the x and y transitions can be degenerate or non-degenerate in energy;

230 (3) The x and y transitions of the same band must have equal linewidths, but their
231 intensity ratio may vary;

232 (4) Bands in 500-580 nm region are approximated by two gaussians of variable
233 linewidths.

234 The reconstructed heme a^{2+} Soret band with a maximum at 447.5 nm is symmetric and
235 much narrower than reported by Vanneste (full width at half-height (FWHH) 18 nm vs 24 nm,
236 correspondingly [11]). It is described by the sum (**Fig. 2c**, red) of two gaussians of equal
237 FWHH of 15 nm at 442 nm and 450 nm, and an additional minor component at 420 nm with a
238 FWHH of 18 nm (red dotted). We assign the gaussians at 442 and 450 nm to two non-
239 degenerate B_y and B_x electronic transitions in heme a^{2+} , split by 8 nm, respectively.

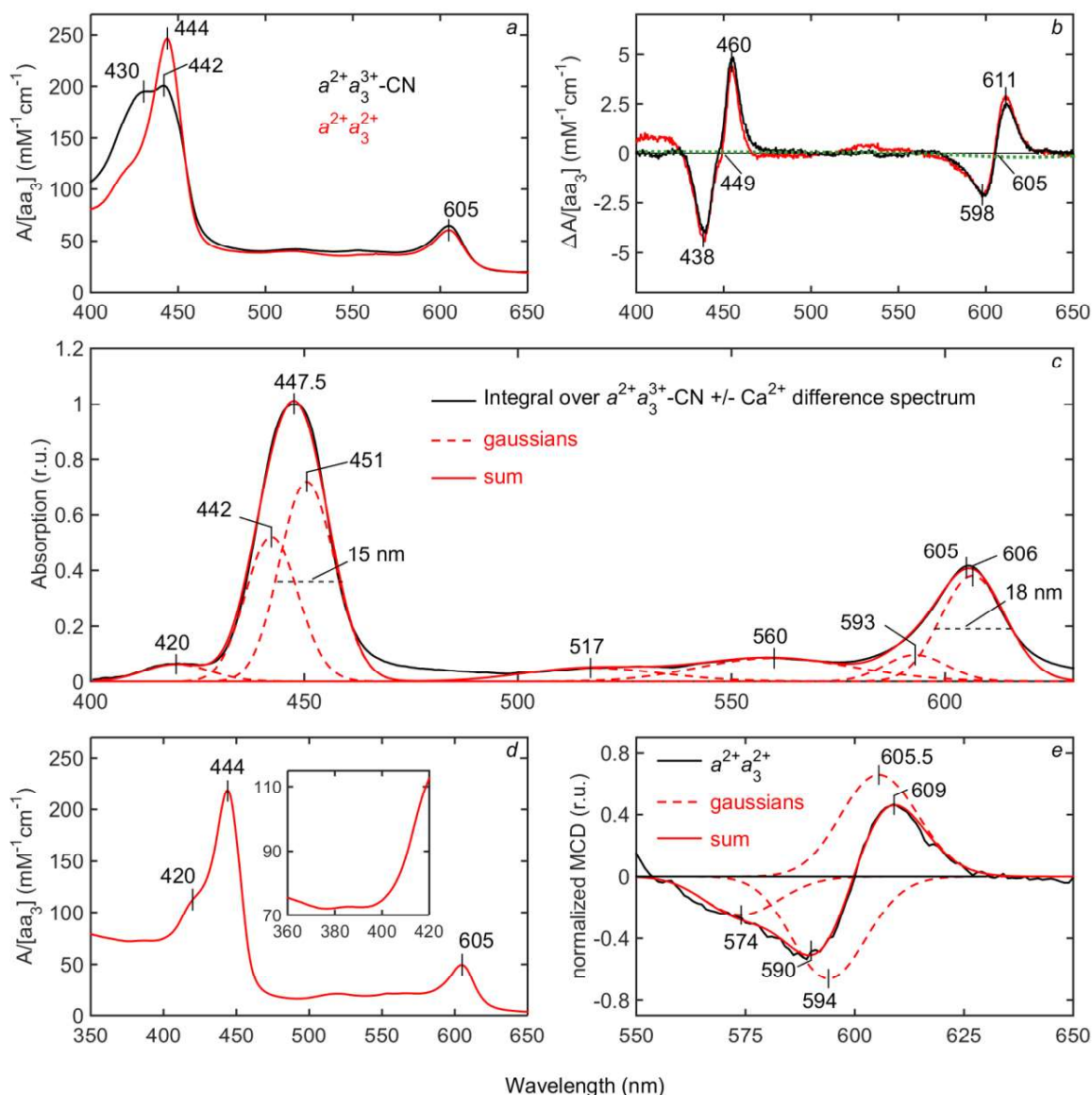
240 Short-wavelength components of the heme a^{2+} Soret band could reside, in principle,
241 below 420 nm. However, most conventional reductants such as dithionite or ascorbate
242 strongly absorb in the near-UV possibly masking these spectral components. We therefore
243 attempted to obtain a “clean” spectrum of CcO in the Soret band by bubbling gaseous
244 hydrogen *in statu nascendi* released by sodium borohydride through the anaerobic solution of
245 the oxidized enzyme. Hydrogen bubbling resulted in partial (~85%) CcO reduction. The H₂-
246 reduced CcO spectrum corrected for the fraction of the oxidized form (**Fig. 2d**) reveals no
247 additional spectral components below 420 nm.

248 The splitting of the Soret band of heme a^{2+} implies that the α -band of the heme should
249 similarly contain split x- and y- components [29]. The α -band differential Ca²⁺-induced
250 spectrum shows certain asymmetry (**Fig. 2b**), and, consistently, the reconstructed α -band

251 (maximum at 605 nm, FWHH 21 nm) has somewhat extended short wavelength side. The α -
252 band fitting requires two gaussians of 17-18 nm FWHH separated by 13 nm (at 593 nm and
253 606 nm). However, in variance with the Soret band, the x and y components of the Q_0 -band
254 differ much in intensity, so that the overall maximum at 605 nm almost coincides with the
255 maximum of the dominating Q_{0x} -transition at 606 nm.

256 To further explore the proposed Q_0 -band splitting, we recorded room temperature
257 magnetic circular dichroism (MCD) spectrum of our CcO preparation in the visible range (**Fig.**
258 **2e**, black). The spectrum with positive and the negative lobes at 609 nm and 590 nm and
259 zero-crossing at 600 nm is very close to that in [29], except for a slight shift of our spectrum to
260 the red. The MCD spectrum decomposes into a sum of two gaussians of equal magnitude
261 and width but of opposite sign corresponding to the individual heme a^{2+} Q_{0x} and Q_{0y} terms,
262 and a third negative gaussian at 574 nm (**Fig. 2e**, red dashed: gaussians, red solid: their
263 sum). The extrema of the two components are observed at 594 (min) and 605.5 nm (max),
264 *i.e.*, very close to the maxima of the two components fitted to the heme a^{2+} α -band (**Fig. 2c**),
265 supporting their attribution to the Q_{0x} - and Q_{0y} - electronic transitions.

266



26

268

269

270

271

272

273

274

275

276

277

Fig. 2. Reconstruction of the heme a^{2+} absorption spectrum using selective Ca^{2+} -induced spectral shift. (a) Absorption spectra of the bovine CcO: black, mixed-valence CN-complex $a^{2+}a_3^{3+}$ -CN; red, fully reduced unliganded enzyme $a^{2+}a_3^{2+}$. To obtain the mixed-valence CN-complex, “activated” (see 2.1) CcO (1.7 μM) in the basic medium was incubated for 10 minutes with 4 mM KCN and then reduced by 5 mM Tris-ascorbate in the presence of 100 μM TMPD. To produce fully reduced form, CcO was incubated with 5 mM ascorbate and 50 μM RuAm, in a cell covered by a gastight cap. Anaerobic condition followed by full enzyme reduction were achieved after 5-min incubation. (b) Difference spectra of the Ca^{2+} -spectral shift of heme a . The curves show the difference between the absolute spectra of the CcO mixed-valence CN-complex (black) or fully reduced form (red) after the addition of 0.1 mM

278 CaCl₂ and after the subsequent addition of 1 mM EGTA. With the adventitious calcium in the
279 buffer (~ 30 μM), the Ca²⁺ concentration after CaCl₂ addition was ~130-fold the K_d value [26],
280 i.e., sufficient to saturate the calcium binding site. (c) Reconstructed lineshape of the heme
281 a²⁺ absorption spectrum. Black, integral over the black curve in *b*. Red, its approximation by
282 the sum of seven gaussians (dashed red). (d) H₂-reduced bovine CcO absorption spectrum
283 corrected for the contribution (~15%) of resting oxidized form. The spectrum shows no
284 additional shoulder below 420 nm. *Insert*: zoom of the 360-420 nm region. (e) Black, MCD
285 spectrum of reduced bovine CcO. Red, its approximation with 3 gaussian components
286 (dashed red). To obtain reduced CcO, 50 μM Ru(NH₃)₆³⁺ and 5 mM ascorbate was added to
287 12 μM CcO in 0.1M HEPES pH 8.1 with 0.1 mM of added Ca²⁺, 5 minutes prior to the
288 recording of the spectrum.

289

290

291 3.2. *Individual spectra of hemes in the T. thermophilus ba₃ and mitochondrial aa₃ CcO*
292 *resolved with photoexcitation spectroscopy.* Independently, we employed a selective
293 photobleaching approach [30–33] by exciting the hemes by a femtosecond light pump pulse
294 in the Q band to transiently depopulate the electronic ground state and thus to bleach the
295 corresponding ground state-based absorption. Spectral changes were followed using a white
296 continuum probe pulse. Since both Q and B bands originate from the same ground state,
297 excitation in the Q-band bleaches in the Soret as well. Wide separation of the two bands
298 prevents interference of the relatively narrow pump pulse in the Q-band with the probe pulses
299 in the Soret.

300 However, the heme a^{2+} and heme a_3^{2+} Q-band overlap and finite intrinsic width of the
301 pump pulses complicates selective excitation of one heme. Therefore, we turned initially to *T.*
302 *thermophilus ba₃-type CcO* belonging to the same heme-copper superfamily as the *aa₃-type*
303 *oxidases* but with heme *b* instead of heme *a*. In the *ba₃-type CcO*, the Q-bands of high-spin
304 heme a_3^{2+} (~613 nm) and low-spin heme b^{2+} (559 nm) are separated better than the Q-bands
305 of bovine CcO hemes *a* and a_3 (**Fig. 3a,b**). The Soret bleaching only occurs if the pump pulse
306 overlaps with the visible absorption bands. Pumping at 570 nm is expected to excite both
307 hemes and results in photobleaching spectrum with maximum at 426 nm (heme b^{2+} band)
308 with a weak feature at 443 nm (putative heme a_3^{2+} band) (**Fig. 3c**). In contrast, the pump
309 pulse at 623 nm (“623exc” condition) (**Fig. 3b**, red) is expected to selectively excite heme a_3^{2+}
310 since it does not overlap with the heme b^{2+} narrow α -band at 559 nm. Compared to the
311 spectrum of heme a^{2+} in the bovine CcO (**Fig. 2c**), 623exc photobleaching spectrum (**Fig. 3d**)
312 is blue-shifted and strongly asymmetric with extended decay on the high-energy side. Besides
313 two equal-width (12 nm) gaussians at 435 and 444 nm assigned to the purely electronic B_{0y} -
314 and B_{0x} - transitions, the fitting requires a wider band at ~427 nm that may represent the sum
315 of vibronic components. The absence of 623exc photobleaching of *Bacillus subtilis* reduced
316 succinate: menaquinone reductase (SMR) containing heme *b* as the only bleaching target
317 [34] rules out potential heme *b* contribution to this 427-nm band (**Fig. 3d**).

318 Due to spectral overlap, the photobleaching of individual *aa₃ CcO* hemes cannot be
319 resolved with single excitation. We therefore used three excitation wavelengths to vary the
320 heme a^{2+} vs heme a_3^{2+} excitation degree. **Fig. 4a** shows dithionite-reduced *aa₃*
321 photobleaching spectra obtained by excitation with pump pulses centered at 570, 608 and
322 623 nm (“570exc”, “608exc” and “623exc”). The 608exc spectrum qualitatively resembles the
323 CcO photobleaching spectrum reported recently for a similar pump-probe protocol with the

324 excitation at 600 nm [35,36]. The “570exc”, “608exc” and “623exc” spectra differ in amplitude
 325 since the photoexcitation yield depends on the absorption strength in the region of excitation
 326 and on the pump energy. However, their lineshapes also differ, suggesting varying degree of
 327 a^{2+} vs. a_3^{2+} excitation selectivity. The 623exc lineshape is almost symmetrical with a minor
 328 shoulder below 430 nm. The shoulder contributes more to 608exc and especially 570exc
 329 spectra. The maximum of the 570exc spectrum is slightly blue-shifted (see **Fig. 4a**, color
 330 traits). As the heme a_3^{2+} ground state absorption spectrum is blue-shifted relative to heme a^{2+}
 331 spectrum (cf. **Fig. 2c** and **Fig. 3d**), the blue shift of the maximum on the 570exc spectrum
 332 provides a first indication that heme a_3^{2+} contributes more to the 570exc spectrum than to the
 333 608exc and 623exc spectra.

334 To estimate the excitation selectivity, we convoluted the pump pulse positions with the
 335 Q-bands of the hemes a^{2+} and a_3^{2+} (**Fig. 4b**). The spectrum reconstructed from the Ca^{2+} -
 336 induced shift assay was used to model the heme a^{2+} Q-band, assuming that heme a^{2+}
 337 contributes about 80% of absorption in the α -band maximum. The heme a_3^{2+} Q-band was
 338 modeled by subtraction of the heme a^{2+} spectrum from the smoothed aa_3 Q-band. The
 339 resulting a_3^{2+} spectrum has a maximum at ~600 nm and a shoulder below 580 nm, consistent
 340 with the reduced minus oxidized heme a_3 spectrum [37] (see also **Fig. A.5**). We then
 341 estimated the heme a^{2+} vs. heme a_3^{2+} selectivity as the convolution of the pulse profile with
 342 the heme a^{2+} absorption band divided by a convolution of the same pulse profile with the
 343 heme a_3^{2+} absorption band:

$$344 \quad a : a_3 \text{ selectivity} = \frac{\int I_a(\omega) I_{pulse}(\omega)}{\int I_{a_3}(\omega) I_{pulse}(\omega)} \quad (1)$$

345 where I_a and I_{a_3} are heme a^{2+} and heme a_3^{2+} Q-bands, respectively, I_{pulse} is the
 346 corresponding pump pulse profile (570exc, 608exc or 623exc), and the integrals are taken
 347 over the 15391-19992 cm^{-1} spectral range (500-650 nm).

348 The estimated a^{2+} vs. a_3^{2+} excitation yield ratios (**Fig. 4b**) suggest a higher contribution
 349 of heme a^{2+} to the photobleaching spectra at 623exc and 608exc and approximately equal
 350 a_3^{2+} and a^{2+} contributions at 570exc. However, under any excitation conditions, it was not
 351 possible to assign the photobleaching spectra entirely to either heme a^{2+} or a_3^{2+} . To extract
 352 “pure” hemes a^{2+} and a_3^{2+} spectral lineshapes we performed simultaneous decomposition of
 353 the photobleaching spectra obtained at all three excitations (**Fig. 4c-e**) with the following
 354 constraints:

355

356 .(1) The Soret (B -) band of each heme is modeled by 3 gaussian components: two electronic
357 transitions (B_{0x} - and B_{0y} -) with equal widths plus a putative vibronic satellite of variable width.
358 The three gaussians describing heme a^{2+} and heme a_3^{2+} contributions are shown in **Fig. 4c-e**
359 by orange and green, respectively.

360 (2) Position and bandwidth in cm^{-1} (but not amplitude) of a specific transition within a
361 heme is identical for all three photobleaching spectra. For example, the heme a^{2+} B_{0x} -
362 associated gaussians are centered at the same wavelength and have the same width in each
363 of the three sets of gaussians but may differ in amplitude.

364 (3) The resulting shape of the spectrum of an individual heme (a^{2+} or a_3^{2+}) is preserved
365 across the excitation conditions. For example, the sums of the three gaussians attributed to
366 heme a^{2+} have the same lineshape for each of the three sets of gaussians but may differ in
367 amplitude.

368 (4) The photoinduced absorption is simulated by two negative gaussians, one at either
369 side of the spectra, whose positions and bandwidths in cm^{-1} were identical across the
370 excitation conditions.

371 The “pure” normalized heme a^{2+} photobleaching spectrum (**Fig. 4f**, solid orange) is in
372 agreement with the spectrum obtained using Ca^{2+} -induced shift approach (**Fig. 4f**, gray, same
373 as **Fig. 2c**, black). It reveals almost symmetrical lineshape with minor shoulder at 421 nm and
374 contains two individual gaussian components with maxima at 442.5 nm and 450 nm, with a
375 bandwidth of 14 nm each. In contrast, the “pure” normalized heme a_3^{2+} photobleaching
376 spectrum (**Fig. 4g**) has a pronounced shoulder described by 423 nm band with a 25 nm
377 width. In both hemes a and a_3 , the B_x - and B_y - electronic transitions are separated by ~ 8 nm.

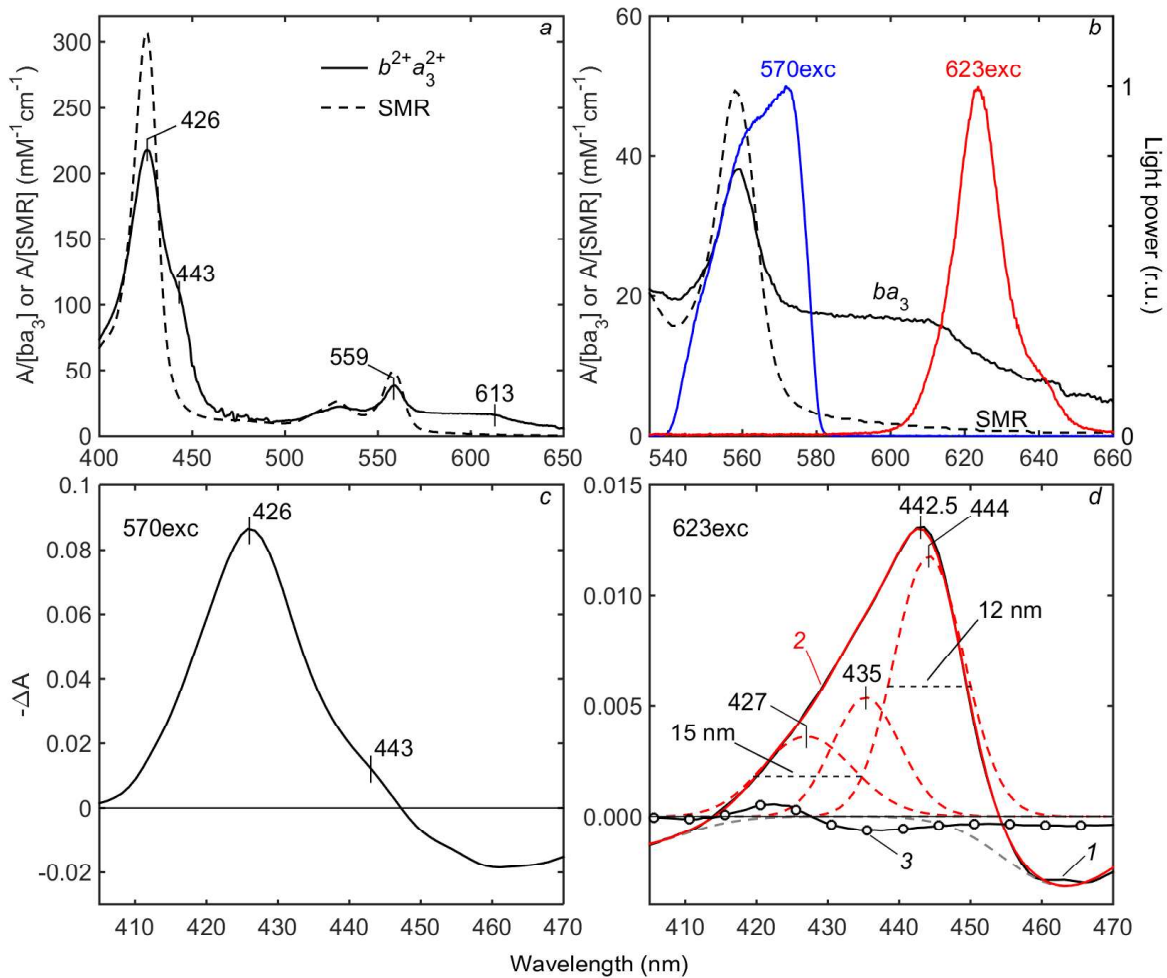
378 As a consistency check, we attempted to reconstruct the overall $a^{2+}a_3^{2+}$ Soret band as a
379 weighted sum of the individual a^{2+} and a_3^{2+} contributions. First, we estimated the proportion of
380 the heme a^{2+} vs. heme a_3^{2+} contribution by assuming that the $a:a_3$ excitation selectivity is
381 most reliably estimated for 608exc condition, where the pumping is close to the heme a^{2+}
382 band maximum (**Fig. 4b**). Selectivity modeling suggests that pumping at 608 nm excites
383 heme a^{2+} 3.15 times stronger than heme a_3^{2+} . At the same time, the ratio of the areas under
384 the sum of the gaussians attributed to heme a^{2+} (orange) to that under the sum of the
385 gaussians attributed to heme a_3^{2+} (green) on the 608exc is not 3.15:1 but 1.70:1 (**Fig. 4d**).
386 This could mean that the contributions of the two hemes to the total extinction are not 1:1 but
387 rather 0.54:1 (heme a^{2+} : 35%, heme a_3^{2+} : 65%). The ratio of the areas under the sums of the
388 heme a^{2+} and heme a_3^{2+} -assigned gaussians for 570exc and 623exc fits (predicted

389 selectivities 0.77 and 4.95, respectively) are 0.58:1 and 2.55:1. This gives the following
390 estimates of the hemes' contributions to the extinction: 43% (heme *a*) and 57% (heme *a*₃) for
391 570exc fit; 34% (heme *a*) and 66% (heme *a*₃) for 623exc fit. The both estimations are fairly
392 close to that obtained above for the 608exc data which confirms the consistency of our
393 modeling.

394 Finally, we obtained the reconstructed *aa*₃ Soret lineshape (**Fig. 4h**, red) by adding the
395 normalized heme *a*²⁺ spectrum multiplied by 0.54 to the normalized heme *a*₃²⁺ spectrum
396 multiplied by 1, and normalizing the sum to its maximum. For comparison, the dithionite-
397 reduced *aa*₃ spectrum is shown, also normalized to its maximum (**Fig. 4h**, gray). The
398 reconstructed Soret lineshape reproduces the position of the maximum and the shoulder at
399 the short-wavelength side. We then investigated whether scattering may explain higher
400 experimental absorption below 430 nm compared to the reconstructed spectrum. For this, we
401 added $\sim\lambda^{-4}$ absorption (**Fig. 4h**, dotted dark red curve) to the sum of *a*²⁺ and *a*₃²⁺ bands. The
402 maximum-normalized resulting spectrum (**Fig. 4h**, dotted blue curve) is fairly close to the
403 experimental Soret lineshape. The remaining differences between the reconstructed band
404 and the experimental *a*²⁺*a*₃²⁺ spectrum can be due to imprecise description of the vibronic
405 satellite(s) by unique gaussian band, unaccounted higher-energy heme transitions, and the β -
406 band tails. Attempting more precise Soret band reconstruction, as well as determination of
407 absolute heme absorbance values, is out of the scope of the present work.

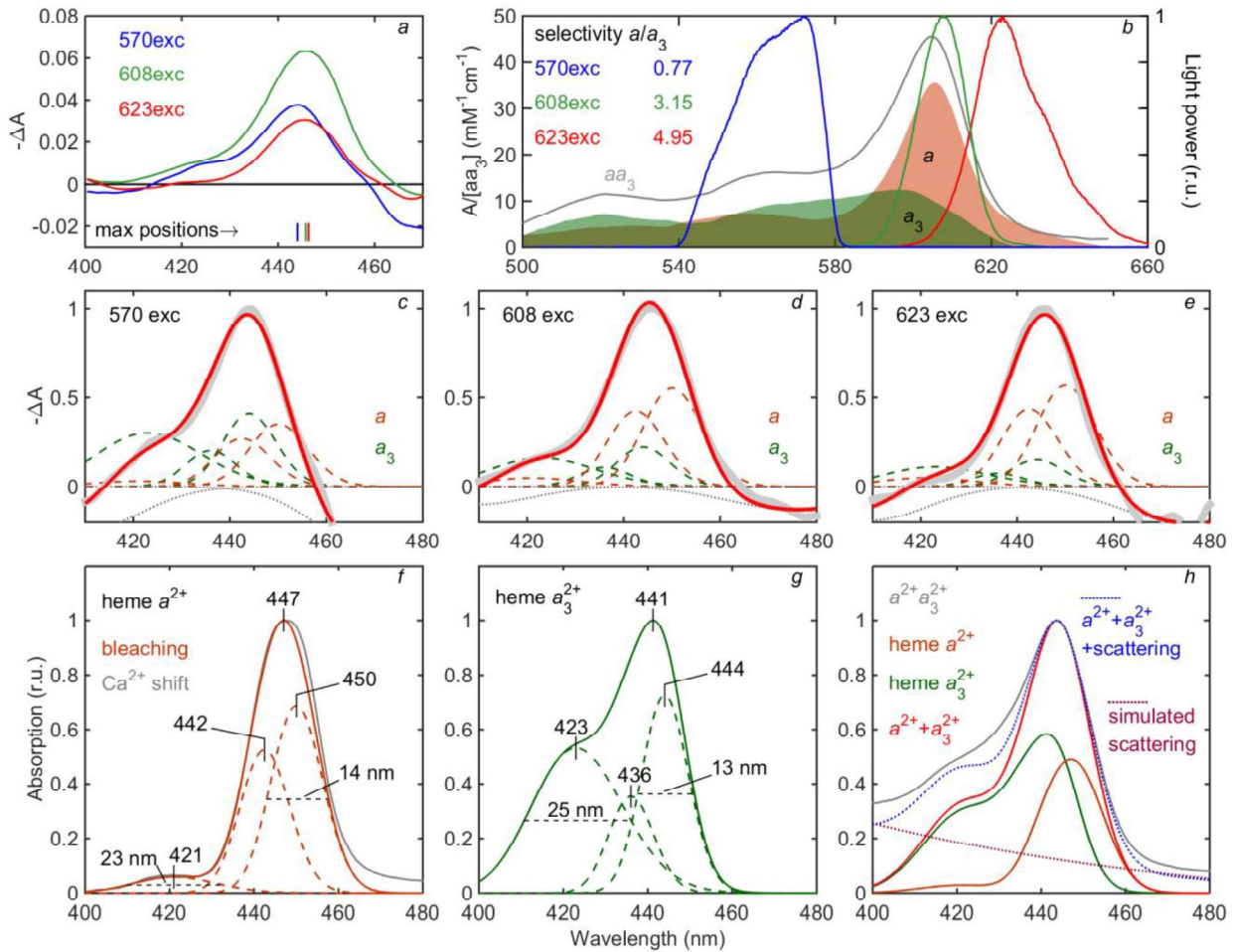
408

409



410
 411 **Fig. 3. Photobleaching of reduced ba_3 CcO from *T. thermophilus*.** (a) Dithionite-reduced
 412 *T. thermophilus* ba_3 (7.9 μM ; solid) and *Bacillus subtilis* succinate: menaquinone reductase
 413 (SMR, 4.1 μM ; dashed) absorption spectra. (b) Pump laser pulse profiles (right vertical axis)
 414 centered at 570 nm (blue) and 623 nm (red) relative to the α -band of the reduced ba_3
 415 spectrum (black, left vertical axis). The *B. subtilis* SMR spectrum (dashed) does not overlap
 416 with the 623exc pulse profile suggesting that heme b^{2+} is not excited by this pulse. (c,d)
 417 Inverted fastest EASs after pumping at 570exc and 623exc, respectively. In d, Curve 1 (solid
 418 black), experimental spectrum that has been fitted by 5 gaussians. The 3 positive gaussians
 419 (dashed red) are assigned to heme a_3^{2+} photobleaching. Two negative gaussians (dashed
 420 gray) approximate the increase of absorption following the excitation that likely represent the
 421 contribution of the electronically excited states (typically weak and diffuse) [38–40]. Curve 2
 422 (solid red) shows the sum of the 5 gaussians mostly coinciding with the experimental curve 1.
 423 Curve 3 (black with open circles), control experiment showing that heme b^{2+} in *B. subtilis*
 424 SMR is not photobleached by excitation at 623 nm.

426
427



428
429

Fig. 4. Photobleaching of reduced bovine CcO. (a) Inverted fastest EASs after pumping at 570, 608 and 623 nm. The traits at the bottom show corresponding maxima positions. (b) Heme a^{2+} vs. heme a_3^{2+} excitation selectivity estimation. Heme a^{2+} spectrum (red area) reconstructed from the Ca^{2+} -induced shift (Fig. 2c) was subtracted from the smoothed reduced aa_3 spectrum (gray) to model heme a_3^{2+} spectrum in the visible range (green area). Heme a^{2+} was assumed to provide ~80% absorption at the α -band maximum. The pump pulse profiles for 570exc, 608exc and 623exc are shown in blue, green and red, respectively. Excitation selectivity was estimated using Eqn (1). (c-e) Approximation of the EASs (thick gray lines) by sets of 6 positive (dashed) and 2 negative (dotted) Gaussians. In each fit, three positive Gaussians were attributed to heme a_3^{2+} (green) and the other three to heme a^{2+} (orange). The two negative Gaussians describe photoinduced absorption. The sum of the Gaussians is shown by a solid red line. (f,g) Heme a^{2+} and heme a_3^{2+} Soret lineshapes (solid lines) determined from the EASs fitting as sums of the three corresponding Gaussians

442 (dashed lines). The lineshapes are normalized to their maxima. In *f*, heme a^{2+} Soret lineshape
443 determined with Ca^{2+} -induced shift technique (gray) is shown for comparison. (*h*) Bovine
444 $a^{2+}a_3^{2+}$ Soret lineshape reconstruction. The ratio of the areas under scaled Soret bands of
445 hemes a^{2+} and a_3^{2+} (orange and green) was estimated to be $a^{2+}:a_3^{2+}=0.54:1$ (see Section
446 3.2). Red, the sum of the individual a^{2+} and a_3^{2+} contributions normalized to its maximum.
447 Dotted dark red, simulated $\sim\lambda^{-4}$ scattering. Dotted blue, the sum of reconstructed a^{2+} and a_3^{2+}
448 bands and the scattering normalized to its maximum. Gray, Soret band of the dithionite-
449 reduced bovine CcO normalized to its maximum.

450 4. Discussion

451 **Table 1** resumes heme a^{2+} and a_3^{2+} spectral properties reported here and compares
452 them with previous studies. Only two papers treat explicitly the lineshape of the absolute
453 spectra of bovine CcO hemes a^{2+} and a_3^{2+} : Vanneste's [11] and Orii's [13]. Our spectra
454 coincide with neither of the two reports but would appear closer to Orii's conclusions.
455 However, the latter depend critically on the choice of the model parameters and can be
456 converted into Vanneste's attributions by changing the baseline slope (**Fig. A.2**). It has been
457 shown by using improved reduction technique that Vanneste's heme a_3 spectra need to be
458 corrected at least in the α -region [37]. In the following we will discuss the spectral properties
459 of the two hemes in detail.

460 *4.1. Soret splitting.* Both hemes a^{2+} and a_3^{2+} showed split Soret bands with B_{0x} - and B_{0y} -
461 components separated by 8-9 nm and close electronic transition widths. The heme a^{2+} Soret
462 band splitting has been inferred earlier [28,29,41–43], but sometimes misinterpreted as
463 evidence for two heme a conformations [42]. The hemes a and a_3 in CcO have the same
464 chemical structure - heme A, - but differ in the protein surroundings and in iron coordination.
465 Therefore, the simplest explanation is that the similar splitting observed for the two hemes is
466 intrinsic to heme A structure. Indeed, the electronic transition along the pyrrole II \rightarrow pyrrole IV
467 axis with the two electron-withdrawing substituents (vinyl and formyl) should differ in energy
468 from the perpendicular transition along the pyrrole I \rightarrow pyrrole III axis with electron donating
469 substituents (methyl, propionate, hydroxyethylfarnesyl group). Conversion of the formyl
470 substituent to the Schiff-base results in drastic narrowing of the heme A Soret band [44] (see
471 also **Fig. A.3**) suggesting restoration of degeneracy or at least reduction of splitting. Inherent
472 heme A splitting is supported by the MCD spectrum of the bis-1-methyl imidazole-6c complex
473 of heme A^{2+} showing the same lineshape (except for the position) as the CcO heme a^{2+} MCD
474 spectrum [29]. However, it seemingly contradicts the absorption spectra second derivative
475 analysis (cf. [41] and refs. therein) suggesting that the Soret splitting is specific for heme a^{2+}
476 in CcO and is not observed in the hexacoordinate (6c-) low-spin (ls-) complexes of isolated
477 heme A^{2+} nor in non- aa_3 -CcO proteins reconstituted with heme a .

478 To clarify this issue, we first tested whether deconvolution into gaussians can reveal the
479 Soret splitting of the isolated heme A^{2+} spectrum by analyzing the bis-imidazole-heme A^{2+}
480 spectra reported in [44]. The ls-6c-heme A^{2+} spectra in solution are broader than in CcO (35
481 nm in aqueous buffer or 27 nm in CH_2Cl_2 vs 18 nm in the CcO protein) and, at this width,
482 single- and two-gaussian approximations (both including one additional gaussian describing a

483 vibronic shoulder) are equally valid (**Fig. A.3**). Further, simple modeling (**Fig. A.4**) shows that
484 the ~10-nm splitting of two gaussians with equal heights and widths typical for CcO requires
485 their FWHH being below ~8 nm to be detected on the second derivative curve. The exact
486 lineshape of the second derivative depends also on the relative heights of the two gaussians.
487 Thus, the second-derivative method may resolve the B_{0x} and B_{0y} bands of heme *a* in the CO-
488 complex of reduced CcO, with heme a_3 bands shifted far to the blue (cf. Fig. 1B in [41]) and to
489 a lesser extent in the fully reduced CcO (Fig. 1A in ref. [41]), but is not expected to resolve the
490 B_{0x} - and B_{0y} - bands in the broad spectra of the isolated 6c-heme A^{2+} .

491 The same applies to the recent second-derivative analysis of the Soret CcO spectra
492 confirming ferrous heme *a* Soret splitting but arguing against splitting of the ferric hemes *a*
493 and a_3 Soret bands [45]. On this basis, the authors proposed that the ferric hemes are
494 symmetric but their reduction changes the protein conformation distorting heme planes and
495 splitting the B_{0x} - and B_{0y} -transitions. However, the Soret bands of the ferric hemes are known
496 to be broader than those of the reduced hemes and their splitting may be unresolved by the
497 second derivative assay.

498 We conclude that although not detectable by second-derivative analysis, the inherent
499 splitting of the heme A^{2+} Soret band is in the origin of the Soret band splitting of both hemes
500 a^{2+} and a_3^{2+} .

501 **4.2. Heme a^{2+} α -band splitting.** Spectral forms of heme a^{2+} differing in the α -peak were
502 described [46,47] but the possibility of a split α -band of the heme was not considered in these
503 studies. Our analysis revealed the presence of a second minor component at 593 nm in
504 addition to the dominating band at 606 nm (**Fig. 2c**). Their attribution to the split Q_{0y} and Q_{0x}
505 bands of heme a^{2+} , respectively, is supported by MCD spectroscopy that allows for better
506 resolution of the split bands. The α -band heme a^{2+} MCD spectrum can be interpreted as a
507 sum of two opposite B-terms belonging to the Q_{0x} and Q_{0y} transitions in heme a^{2+} [29]. The
508 MCD spectrum of our preparation is indeed described as the sum of two identical B-terms of
509 opposite signs (**Fig. 2e**).

510 The Soret splitting is more extensive than that of the α -band (381-416 vs 373 cm^{-1})
511 probably due to the larger Soret vs α -band transition moment implying stronger interaction
512 with the permanent local electric field [48]. In contrast to the Soret where the B_{0x}/B_{0y} intensity
513 ratio is about 1.4 (see **Table 1**), the Q_{0y} band at 593 nm is much weaker than the Q_{0x}
514 component at 606 nm (absorption intensity ratio Q_{0x}/Q_{0y} is ~4). The weaker high-energy (y)
515 Q_0 -component is typical of metal-porphyrin compounds with split absorption bands [49–53]

516 and agrees with calculations [50,54]. Therefore, the commonly observed α -peak of heme a^{2+}
517 at 605 nm largely corresponds to the Q_{0x} transition of the iron-porphyrin ring of heme a^{2+} .

518 **4.3. Position of the Soret absorption peaks of the hemes a^{2+} and a_3^{2+} .** It is commonly
519 assumed that the Soret absorption maxima of hemes a^{2+} and a_3^{2+} are close to each other
520 (Vanneste: 444 nm a^{2+} vs 443 nm a_3^{2+} [11]; Orii: 445 nm a^{2+} vs 443 nm a_3^{2+} [13]). This fact
521 has been long considered surprising in view of the difference in iron coordination and heme-
522 protein interaction.

523 Our data, in contrast, suggest that the Soret maxima (447-447.5 nm a^{2+} vs 441 nm a_3^{2+})
524 and the B_{0x} -, B_{0y} -transition energies of hemes a^{2+} and a_3^{2+} do actually differ. The heme a_3^{2+}
525 B_{0x} - and B_{0y} -transitions are shifted by 6-7 nm to the blue relative to the corresponding
526 transitions of heme a^{2+} , in agreement with the blue shift of the reduced minus oxidized
527 difference spectrum of CcO heme a_3 relative to that of heme a [37]. In apparent contradiction,
528 Soret maxima of high spin mono-His-coordinated (5c-hs) cytochromes b are usually situated
529 to the red from those of low spin, bis-His-coordinated (6c-ls) cytochromes b (**Table A.1**).
530 Congruently, the wide α -band of 5c-hs 1,2-diMelm-heme A^{2+} (heme a_3^{2+} model) locates to the
531 red of the α -band of 6c-ls bis-1-Melm-heme A^{2+} (heme a^{2+} model) [29,41,44]. The inverted
532 maxima positions in CcO may be explained by the opposite shifts of the CcO hemes relative
533 to the corresponding isolated complexes. The spectrum of CcO heme a^{2+} is red-shifted by 9-
534 11 nm in the Soret and by 12-16 nm in the α -band compared to the 6c-ls bis-1-Melm-heme
535 A^{2+} (**Table 1**). This shift is probably induced by a strong hydrogen bond between the in-plane
536 oriented heme a formyl group and the conserved arginine R38_{bt} as proposed originally in [55]
537 and confirmed by mutagenesis of the homologous arginine in bacterial CcOs [56,57]. Indeed,
538 the replacement of the homologous arginine to methionine causes a 605 nm to 589 nm shift
539 of the α -band that would correspond to ~ 10 nm shift in the Soret [56]. On the other hand, the
540 reduced *minus* oxidized difference spectrum of the CcO heme a_3 appears to be blue-shifted
541 by about 7 nm compared to that of 5c-hs heme A^{2+} while preserving the spectral shape ([37];
542 **Fig. A.5**) suggesting ~ 3 -4 nm blue shift in the Soret.

543 **4.4. B-band short-wavelength shoulder.** Heme a_3^{2+} shows a pronounced high-energy
544 shoulder of the Soret peak (**Fig. 4g**), presumably a vibronic satellite of the B_0 transitions.
545 Isolated 6c-ls heme A^{2+} also exhibits a shoulder ([44]; **Fig. A.3a,b**). However, no vibronic
546 satellite can be seen in the spectrum of heme a^{2+} in CcO, except for a tiny band at 420-421
547 nm (**Fig. 2c, 4f**). The vibronic β -band shows two peaks at ~ 517 nm and ~ 560 nm. The one at
548 ~ 517 nm [11] or both peaks [58] were attributed to heme a^{2+} features. Both peaks are red-

549 shifted by Ca^{2+} and appear in the integral of the Ca^{2+} -induced difference spectrum (**Fig. 2c**).
550 The first vibrational progression peak, if any, of the a^{2+} B band would therefore be expected at
551 1500 cm^{-1} higher energy than the electronic peak, i.e., at $\sim 419\text{ nm}$. Therefore, the small 420-
552 nm band in the reconstructed heme a^{2+} spectrum could indeed indicate the presence of a
553 strongly dampened vibronic mode. The reason of the dampening is not yet clear. However,
554 the nearly symmetric lineshape of the heme a^{2+} spectrum is consistent with Soret spectra of
555 other reduced 6c-Is cytochromes, for example, cytochrome c_5 [59–61], neuroglobin [62–66],
556 cytochrome b_{559} [62], superoxide dismutase [62], cytochrome b_{560} [67], cytoglobin [68], and
557 SMR (**Fig. 3a**). The absence of the shoulder in the spectrum of the 6c-Is heme integrated into
558 the protein could be explained by silencing of the corresponding heme plane vibrations by
559 axial histidines attached to the polypeptide backbone so that out-of-plane movements may be
560 restricted. Heme a_3^{2+} and the free bis-imidazole 6c-Is heme A^{2+} would have this vibrational
561 mode permitted because the heme is either attached to only one histidine or to axial
562 imidazoles that are not connected to any larger scaffold.

563 *4.5. Conclusion and outlook.* Upon reinvestigating the decomposition of the reduced aa_3
564 optical absorption spectrum we propose different contributions of the a and a_3 hemes that
565 may resolve long-lasting confusion in the literature. We foresee that this work will be valuable
566 for (re-evaluation of) spectroscopic studies of the CcO mechanism. Extension of our approach
567 may come from polarization-sensitive studies in particular on macroscopically ordered
568 systems and true 2-dimensional pump-probe approaches.

569

570 **5. Acknowledgments**

571 Funding: This work was supported by Howard Hughes Medical Institute Award [grant
572 number #55005615] (to AK) and RFBR (Russian Foundation for Basic Research) [grant
573 number #17-04-00160] (to AK). The funding sources had no involvement in study design nor
574 in the collection, analysis and interpretation of data nor in the writing of the report nor in the
575 decision to submit the article for publication.

576

577 **6. Data availability**

578 Numeric data and all scripts used to analyze data and produce figures are downloadable
579 from Mendeley Data: <https://data.mendeley.com/datasets/dmrkn9pfr/3> [69].

Table 1. Spectral characteristics of hemes a^{2+} and a_3^{2+} reported in this work and in previous studies

	Soret band					α -band				source	
	overall peak	B_{0y}	B_{0x}	B_{0y} - B_{0x} splitting	B_{0x}/B_{0y} ratio	B_v	overall peak	Q_{0y}	Q_{0x}		Q_{0y} - Q_{0x} splitting
a^{2+} (bovine)	447.5 (18) 22342 (914)	442 (15) 22609 (741)	451 (15) 22193 (741)	8 416	1.4	420 (18) 23808 (1037)	605 (21) 16517 (567)	593 (17) 16862 (489)	606 (18) 16489 (489)	13 373	This work (Fig.2c,4f) (Ca^{2+} -shift)
a^{2+} (bovine)	447 (18) 22346 (880)	442.5 (14) 22599 (705)	450 (14) 22218 (705)	7.5 381	1.3	421 (23) 23753 (1295)					This work (Fig.4f) (a_{a3} photobleaching)
a_3^{2+} (bovine)	441 (30) 22664 (1608)	436 (13) 22936 (659)	444 (13.0) 22523 (659)	8 413	2.0	423 (25) 23641 (1413)					This work (Fig.4g) (a_{a3} photobleaching)
a_3^{2+} (ba_3)	442.5 (19) 22599 (965)	435 (11) 22972 (589)	444 (12) 22515 (589)	9 457	2.2	427 (15) 23419 (824)					This work (Fig.3d) (ba_3 photobleaching)
a^{2+} (bovine)		442-443	450-451	7-9							Fig.1 in [41]
A^{2+} bis-Im in SDS	438 (35) 22831 (1884) extended on blue						593 (39) 16863 (1104)				Fig.6 in [41]
bis-Im A^{2+} Is aqueous buffer	440 (35) 22726 (1841)	436 (22) ^a 22919 (1177)	446 (23) ^a 22428 (1177)	10 ^a 491	1.2 ^a	416 ^a 24033	597 (57) 16750 (1644)				Fig.3B in [44] and Fig. A.3b of present paper
bis-Im A^{2+} Is CH_2Cl_2	438 (27) 22830 (1419)	435 (22) ^a 22989 (1177)	442 (23) ^a 22604 (1177)	7 ^a 385	1.0 ^a	414 ^a 24131	592 (41) 16892 (1182)				Fig.4B in [44] and Fig. A.3d of present paper
Bis- <i>n</i> -butylamine A^{2+} Is Schiff base derivative aqueous buffer	427 (19) 23419 (1023)	425 (16) ^a 23512 (895) 428 (17) ^b 23374 (922)	430 (17) ^a 23256 (895)	5 ^a 256	1.0 ^a	407 ^a 24599 409 ^b 24471	573 (29) 17452 (899)				Fig.3B in [44] and Fig. A.3e,f of present paper
Bis- <i>n</i> -butylamine A^{2+} Is Schiff base derivative CH_2Cl_2	428 (18) 23364 (988)	427 (16) ^a 23398 (875) 429 (16) ^b 23326 (870)	430 (16) ^a 23256 (875)	3 ^a 142	1.0 ^a	410 ^a 24399 411 ^b 24331	575 (31) 17391 (958)				Fig.4B in [44] and Fig. A.3g,h of present paper
Bis-1-Melm A^{2+} Is CH_2Cl_2 (MCD)		430 ^c 23249	442 ^c 22602	12 647			574 ^c 17435	599 ^c 16706	25 729		Fig. 2 in [29]
Bis-1-Melm A^{2+} Is CH_2Cl_2 (absorption)							588 (32) 17001 (935)				Fig. 7 in [29]
1,2-diMelm A^{2+} Is CH_2Cl_2 (absorption)							606 (139) 16500 (4493)				Fig. 7 in [29]

581 Format: position (full width at half-height); upper row: nm, lower row: cm^{-1} ; ^a 3-gaussian fit in Fig. A.4; ^b 2-gaussian fit in Fig. A.4; ^c positions of the two opposite extrema in

582 the MCD spectrum

583
584
585
586
587
588
589
590
591
592
593
594
595
596
597
598
599
600
601
602
603
604
605
606
607
608
609
610
611
612
613
614
615
616
617
618
619
620
621
622
623
624
625
626
627
628
629
630

References

- [1] M. Wikstrom, Proton Pump Coupled to Cytochrome c Oxidase in Mitochondria, *Nature*. 266 (1977) 271–273.
- [2] A.A. Konstantinov, Role of protons in the mechanism of coupling site III of the mitochondrial respiratory chain: cytochrome oxidase as an electronic-protonic generator of membrane potential, *Dokl. Akad. Nauk SSSR*. 237 (1977) 713–716.
- [3] V.Y. Artzatbanov, A.A. Konstantinov, V.P. Skulachev, Involvement of Intramitochondrial Protons in Redox Reactions of Cytochrome a, *FEBS Lett.* 87 (1978) 180–185.
- [4] M. Wikstrom, Cytochrome c oxidase: 25 years of the elusive proton pump, *Biochim. Biophys. Acta.* 1655 (2004) 241–247.
- [5] A.A. Konstantinov, Cytochrome c oxidase: Intermediates of the catalytic cycle and their energy-coupled interconversion, *FEBS Lett.* 586 (2012) 630–639. <https://doi.org/10.1016/j.febslet.2011.08.037>.
- [6] S.A. Siletsky, A.A. Konstantinov, Cytochrome c oxidase: charge translocation coupled to single-electron partial steps of the catalytic cycle., *Biochim. Biophys. Acta.* 1817 (2012) 476–88. <https://doi.org/10.1016/j.bbabi.2011.08.003>.
- [7] S. Yoshikawa, K. Muramoto, K. Shinzawa-Itoh, Proton-pumping mechanism of cytochrome C oxidase., *Annu. Rev. Biophys.* 40 (2011) 205–23. <https://doi.org/10.1146/annurev-biophys-042910-155341>.
- [8] S. Ferguson-Miller, G.T. Babcock, Heme/Copper Terminal Oxidases., *Chem. Rev.* 96 (1996) 2889–2908. <http://www.ncbi.nlm.nih.gov/pubmed/11848844> (accessed September 4, 2013).
- [9] S. Yoshikawa, A. Shimada, Reaction mechanism of cytochrome c oxidase., *Chem. Rev.* 115 (2015) 1936–89. <https://doi.org/10.1021/cr500266a>.
- [10] J.R. Platt, Electronic structure and excitation of polyenes and porphyrins, in: A. Hollaender (Ed.), *Radiat. Biol.*, McGraw-Hill, New York, 1956: pp. 71–123.
- [11] W.H. Vanneste, The Stoichiometry and Absorption Spectra of Components a and a3 in Cytochrome c Oxidase, *Biochemistry.* 65 (1966) 838–848. <http://pubs.acs.org/doi/pdf/10.1021/bi00867a005>.
- [12] M. Wikstrom, K. Krab, M. Saraste, *Cytochrome Oxidase - A Synthesis*, Academic Press, New York, 1981.
- [13] Y. Orii, Determination and Novel Features of the Absolute Absorption Spectra of the Heme a Moieties in Cytochrome c Oxidase, *J. Bioenerg. Biomembr.* 30 (1998) 47–53.
- [14] L.R. Fowler, S.H. Richardson, Y. Hatefi, A rapid method for the preparation of highly purified cytochrome oxidase, *Biochim. Biophys. Acta.* 64 (1962) 170–173.
- [15] T. V Vygodina, A. Kirichenko, A.A. Konstantinov, Cation binding site of cytochrome c oxidase: progress report., *Biochim. Biophys. Acta.* 1837 (2014) 1188–95. <https://doi.org/10.1016/j.bbabi.2014.02.025>.
- [16] T. Soulimane, U. Gohlke, R. Huber, G. Buse, Three-dimensional crystals of cytochrome-c oxidase from *Thermus thermophilus* diffracting to 3.8 Å resolution, *FEBS Lett.* 368 (1995) 132–134. [https://doi.org/10.1016/0014-5793\(95\)00623-H](https://doi.org/10.1016/0014-5793(95)00623-H).
- [17] O. Farver, Y. Chen, J.A. Fee, I. Pecht, Electron transfer among the Cu A -, heme b - and a 3 - centers of *Thermus thermophilus* cytochrome ba 3, *FEBS Lett.* 580 (2006) 3417–3421. <https://doi.org/10.1016/j.febslet.2006.05.013>.
- [18] L. Hederstedt, Cytochrome b reducible by succinate in an isolated succinate dehydrogenase-cytochrome b complex from *Bacillus subtilis* membranes, *J. Bacteriol.* 144 (1980) 933–940. <https://doi.org/10.1128/jb.144.3.933-940.1980>.
- [19] G. Cerullo, S. De Silvestri, Ultrafast optical parametric amplifiers, *Rev. Sci. Instrum.* 74 (2003) 1. <https://doi.org/10.1063/1.1523642>.

- 631 [20] J.J. Snellenburg, S.P. Laptinok, R. Seger, K.M. Mullen, I.H.M. van Stokkum, Glotaran : A Java
632 -Based Graphical User Interface for the R Package TAMP, *J. Stat. Softw.* 49 (2012) 1–22.
633 <https://doi.org/10.18637/jss.v049.i03>.
- 634 [21] R.H. Byrd, M.E. Hribar, J. Nocedal, An Interior Point Algorithm for Large-Scale Nonlinear
635 Programming, *SIAM J. Optim.* 9 (1999) 877–900.
636 <http://epubs.siam.org/doi/abs/10.1137/S1052623497325107> (accessed December 7, 2015).
- 637 [22] R.H. Byrd, J.C. Gilbert, J. Nocedal, A trust region method based on interior point techniques
638 for nonlinear programming, *Math. Program.* 89 (2000) 149–185.
639 <https://doi.org/10.1007/PL00011391>.
- 640 [23] R.A. Waltz, J.L. Morales, J. Nocedal, D. Orban, An interior algorithm for nonlinear optimization
641 that combines line search and trust region steps, *Math. Program.* 107 (2006) 391–408.
642 <https://doi.org/10.1007/s10107-004-0560-5>.
- 643 [24] H. Saari, T. Pentilla, M. Wikstrom, Interaction of Ca²⁺ and H⁺ with heme A in cytochrome
644 oxidase, *J. Bioenerg. Biomembr.* 12 (1980) 325–338.
- 645 [25] H. Mkrtchyan, T. Vygodina, A.A. Konstantinov, Na⁺-induced Reversal of the Ca²⁺-dependent
646 Red Shift of Cytochrome a. Is there a Hydronium Output Well in Cytochrome c Oxidase?,
647 *Biochem. Internat.* 20 (1990) 183–190.
- 648 [26] A. Kirichenko, T. Vygodina, H.M. Mkrtchyan, A. Konstantinov, Specific cation binding site in
649 mammalian cytochrome oxidase., *FEBS Lett.* 423 (1998) 329–33.
650 <http://www.ncbi.nlm.nih.gov/pubmed/9515733> (accessed September 3, 2013).
- 651 [27] M. Wikström, H. Saari, A spectral shift in cytochrome a induced by calcium ions., *Biochim.*
652 *Biophys. Acta.* 408 (1975) 170–9. <http://www.ncbi.nlm.nih.gov/pubmed/811258> (accessed
653 September 3, 2013).
- 654 [28] A. V Dyuba, T. V Vygodina, A.A. Konstantinov, Reconstruction of Absolute Absorption
655 Spectrum of Reduced Heme a in Cytochrome c Oxidase from Bovine Heart, (2013).
- 656 [29] K. Carter, G. Palmer, Models of the Two Heme Centers in Cytochrome Oxidase, *J. Biol.*
657 *Chem.* 257 (1982) 13507–13514. <http://www.jbc.org/content/257/22/13507.full.pdf>.
- 658 [30] J.-L. Martin, M.H. Vos, Femtosecond Biology, *Ann. Rev. Biophys. Biomol. Struct.* 21 (1992)
659 199–222.
- 660 [31] M.H. Vos, Ultrafast dynamics of ligands within heme proteins, *Biochim. Biophys. Acta -*
661 *Bioenerg.* 1777 (2008) 15–31. <https://doi.org/10.1016/j.bbabi.2007.10.004>.
- 662 [32] M.H. Vos, J.L. Martin, Femtosecond processes in proteins, *Biochim. Biophys. Acta - Bioenerg.*
663 1411 (1999) 1–20. [https://doi.org/10.1016/S0005-2728\(99\)00035-3](https://doi.org/10.1016/S0005-2728(99)00035-3).
- 664 [33] M.H. Vos, V.B. Borisov, U. Liebl, J.L. Martin, A.A. Konstantinov, Femtosecond resolution of
665 ligand-heme interactions in the high-affinity quinol oxidase bd: A di-heme active site?, *Proc.*
666 *Natl. Acad. Sci. U. S. A.* 97 (2000) 1554–1559. <https://doi.org/10.1073/pnas.030528197>.
- 667 [34] C. Hägerhäll, C. Von Wachenfeldt, L. Hederstedt, R. Aasa, Two Hemes in *Bacillus subtilis*
668 Succinate : Menaquinone Oxidoreductase (Complex II), *Biochemistry.* 31 (1992) 7411–7421.
669 <https://doi.org/10.1021/bi00147a028>.
- 670 [35] I. V. Shelaev, F.E. Gostev, T. V. Vygodina, S. V. Lepeshkevich, B.M. Dzhagarov,
671 Femtosecond absorption spectroscopy of cytochrome c oxidase: Excited electronic states and
672 relaxation processes in heme a and heme a₃ centers, *High Energy Chem.* 52 (2018) 45–51.
673 <https://doi.org/10.1134/S0018143918010101>.
- 674 [36] I. V. Shelaev, F.E. Gostev, T. V. Vygodina, S. V. Lepeshkevich, B.M. Dzhagarov,
675 Femtosecond Absorption Spectroscopy of Reduced and Oxidized Forms of Cytochrome c
676 Oxidase: Excited States and Relaxation Processes in Heme a and a₃ Centers, *Opt.*
677 *Spectrosc.* 127 (2019) 756–762. <https://doi.org/10.1134/S0030400X19100278>.
- 678 [37] G.L. Liao, G. Palmer, The reduced minus oxidized difference spectra of cytochromes a and
679 a₃, *Biochim. Biophys. Acta - Bioenerg.* 1274 (1996) 109–111. <https://doi.org/10.1016/0005->

- 2728(96)00014-X.
- [38] J.W. Petrich, C. Poyart, J.L. Martin, Photophysics and Reactivity of Heme Proteins: A Femtosecond Absorption Study of Hemoglobin, Myoglobin, and Protoheme, *Biochemistry*. 27 (1988) 4049–4060. <https://doi.org/10.1021/bi00411a022>.
- [39] P. Stoutland, J.-C. Lambry, J.-L. Martin, W.H. Woodruff, Femtosecond Dynamics of reduced Cytochrome Oxidase and its CO derivative, *J. Phys. Chem.* 95 (1991) 6406–6408.
- [40] U. Liebl, G. Lipowski, M. Négrerie, J.-C. Lambry, J.-L. Martin, M.H. Vos, Coherent reaction dynamics in a bacterial cytochrome c oxidase, *Nature*. 401 (1999) 181–184. <https://doi.org/10.1038/43699>.
- [41] J.S. Felsch, M.P. Horvath, S. Gursky, M.R. Hobaugh, P.N. Goudreau, J.A. Fee, W.T. Morgan, S.J. Admiraal, M. Ikeda-Saito, T. Fujiwara, Y. Fukumori, T. Yamanaka, R.A. Copeland, Probing protein-cofactor interactions in the terminal oxidases by second derivative spectroscopy: Study of bacterial enzymes with cofactor substitutions and heme a model compounds, *Protein Sci.* 3 (1994) 2097–2103. <https://doi.org/10.1002/pro.5560031123>.
- [42] D. Sherman, S. Kotake, N. Ishibe, R.A. Copeland, Resolution of the Electronic Transitions of Cytochrome c Oxidase: Evidence for Two Conformational States of Ferrous Cytochrome a, *Proc. Natl. Acad. Sci. USA*. 88 (1991) 4265–4269.
- [43] D. Wilson, M. Gilmour, The low-temperature spectral properties of mammalian cytochrome oxidase. I. The enzyme in intact rat-liver mitochondria, *Biochim. Biophys. Acta - Bioenerg.* (1967). <http://www.sciencedirect.com/sci-hub.io/science/article/pii/0005272867901089> (accessed December 17, 2015).
- [44] S.W. Han, Y.C. Ching, S.L. Hammes, D.L. Rousseau, Vibrational structure of the formyl group on heme a. Implications on the properties of cytochrome c oxidase, *Biophys. J.* 60 (1991) 45–52. [https://doi.org/10.1016/S0006-3495\(91\)82029-X](https://doi.org/10.1016/S0006-3495(91)82029-X).
- [45] K. Kopcova, L. Blascakova, T. Kozar, D. Jancura, M. Fabian, Response of Heme Symmetry to the Redox State of Bovine Cytochrome c Oxidase, *Biochemistry*. 57 (2018) 4105–4113. <https://doi.org/10.1021/acs.biochem.8b00459>.
- [46] M.K. Wikstrom, H.J. Harmon, W.J. Ingledew, B. Chance, A Re-evaluation of the Spectral, Potentiometric, and Energy-Linked Properties of Cytochrome c Oxidase in Mitochondria, *FEBS Lett.* 65 (1976) 259–277.
- [47] M.C. Rocha, R. Springett, Spectral components of detergent-solubilized bovine cytochrome oxidase, *Biochim. Biophys. Acta - Bioenerg.* 1859 (2018) 555–566. <https://doi.org/10.1016/j.bbabi.2018.04.009>.
- [48] E.S. Manas, J.M. Vanderkooi, K.A. Sharp, The Effects of Protein Environment on the Low Temperature Electronic Spectroscopy of Cytochrome c and Microperoxidase-11, *J. Phys. Chem. B.* 103 (1999) 6334–6348. <https://doi.org/10.1021/jp9908552>.
- [49] K.S. Reddy, P.J. Angiolillo, W.W. Wright, M. Laberge, J.M. Vanderkooi, Spectral splitting in the α (Q0.0) absorption band of ferrous cytochrome c and other heme proteins, *Biochemistry*. 35 (1996) 12820–12830. <https://doi.org/10.1021/bi960895l>.
- [50] V. Sanfratello, A. Boffi, A. Cupane, M. Leone, Heme symmetry, vibronic structure, and dynamics in heme proteins: Ferrous nicotinate horse myoglobin and soybean leghemoglobin, *Biopolym. - Biospectroscopy Sect.* 57 (2000) 291–305. [https://doi.org/10.1002/1097-0282\(2000\)57:5<291::AID-BIP60>3.0.CO;2-O](https://doi.org/10.1002/1097-0282(2000)57:5<291::AID-BIP60>3.0.CO;2-O).
- [51] M. Levantino, Q. Huang, A. Cupane, M. Laberge, A. Hagarman, R. Schweitzer-Stenner, The importance of vibronic perturbations in ferrocycytochrome c spectra: A reevaluation of spectral properties based on low-temperature optical absorption, resonance Raman, and molecular-dynamics simulations, *J. Chem. Phys.* 123 (2005) 054508. <https://doi.org/10.1063/1.1961556>.
- [52] J.A. Cowan, H.B. Gray, Q-Band Splitting in the Spectra of Heme Proteins, *Inorg. Chem.* 28 (1989) 4554–4556. <https://doi.org/10.1021/ic00324a026>.

- 729 [53] W.B. Elliott, E. Margoliash, High Resolution Low Temperature Spectrophotometry of
730 Cytochromes c, in: *Dev. Appl. Spectrosc.*, Springer US, 1971: pp. 125–140.
731 https://doi.org/10.1007/978-1-4757-0782-3_5.
- 732 [54] J.A. Shelnut, The Raman excitation spectra and absorption spectrum of a metalloporphyrin in
733 an environment of low symmetry, *J. Chem. Phys.* 72 (1980) 3948.
734 <https://doi.org/10.1063/1.439664>.
- 735 [55] G.T. Babcock, P.M. Callahan, Redox-Linked Hydrogen Bond Strength Changes in
736 Cytochrome a: Implications for a Cytochrome Oxidase Proton Pump, *Biochemistry.* 22 (1983)
737 2314–2319.
- 738 [56] S. Riistama, M.I. Verkhovsky, L. Laakkonen, M. Wikström, A. Puustinen, Interaction between
739 the formyl group of heme a and arginine 54 in cytochrome aa(3) from *Paracoccus*
740 *denitrificans.*, *Biochim. Biophys. Acta.* 1456 (2000) 1–4.
741 <http://www.ncbi.nlm.nih.gov/pubmed/10611451> (accessed September 5, 2013).
- 742 [57] H. Lee, T.K. Das, D.L. Rousseau, D. Mills, S. Ferguson-Miller, R.B. Gennis, Mutations in the
743 Putative H-Channel in the Cytochrome c Oxidase from *Rhodobacter sphaeroides* Show That
744 This Channel Is Not Important for Proton Conduction but Reveal Modulation of the Properties
745 of Heme a †, *Biochemistry.* 39 (2000) 2989–2996. <https://doi.org/10.1021/bi9924821>.
- 746 [58] A. V Dyuba, T. Vygodina, N. Azarkina, A.A. Konstantinov, Calcium ions inhibit reduction of
747 heme a in bovine cytochrome c oxidase., *FEBS Lett.* 589 (2015) 3853–8.
748 <https://doi.org/10.1016/j.febslet.2015.11.023>.
- 749 [59] A.I. Cederbaum, Molecular mechanisms of the microsomal mixed function oxidases and
750 biological and pathological implications, *Redox Biol.* 4 (2015) 60–73.
751 <https://doi.org/10.1016/j.redox.2014.11.008>.
- 752 [60] Y. Yoshida, Y. Tamura-Higashimaki, R. Sato, Purification and characterization of intact
753 cytochrome b5 from yeast microsomes, *Arch. Biochem. Biophys.* 220 (1983) 467–476.
754 [https://doi.org/10.1016/0003-9861\(83\)90437-X](https://doi.org/10.1016/0003-9861(83)90437-X).
- 755 [61] P.L. Holmans, M.S. Shet, C.A. Martin-Wixtrom, C.W. Fisher, R.W. Estabrook, The High-Level
756 Expression in *Escherichia coli* of the Membrane-Bound Form of Human and Rat Cytochrome
757 b5 and Studies on Their Mechanism of Function, *Arch. Biochem. Biophys.* 312 (1994) 554–
758 565.
- 759 [62] M.H. Vos, A. Battistoni, C. Lechauve, M.C. Marden, L. Kiger, A. Desbois, E. Pilet, E. de Rosni,
760 U. Liebl, Ultrafast heme-residue bond formation in six-coordinate heme proteins: implications
761 for functional ligand exchange, *Biochem.* 47 (2008) 5718–5723.
- 762 [63] J.T. Trent III, M.S. Hargrove, A ubiquitously expressed human hexacoordinate hemoglobin, *J.*
763 *Biol. Chem.* 277 (2002) 19538–19545.
- 764 [64] L. Li, H. Ji, C. Zhao, T. Xu, G. Liu, C. Fu, H. Yan, Expression, purification and spectra
765 characterization of neuroglobin, *Chinese Sci. Bull.* 50 (2005) 1708–1713.
766 <https://doi.org/10.1360/982004-618>.
- 767 [65] A. Giuffrè, T. Moschetti, B. Vallone, M. Brunori, Neuroglobin: Enzymatic reduction and oxygen
768 affinity, *Biochem. Biophys. Res. Commun.* 367 (2008) 893–898.
769 <https://doi.org/10.1016/j.bbrc.2008.01.021>.
- 770 [66] K. Nienhaus, G.U. Nienhaus, Probing heme protein-ligand interactions by UV/visible
771 absorption spectroscopy., *Methods Mol. Biol.* 305 (2005) 215–242. [https://doi.org/10.1385/1-](https://doi.org/10.1385/1-59259-912-5:215)
772 [59259-912-5:215](https://doi.org/10.1385/1-59259-912-5:215).
- 773 [67] L. Yu, J.X. Xu, P.E. Haley, C.A. Yu, Properties of bovine heart mitochondrial cytochrome
774 b560, *J. Biol. Chem.* 262 (1987) 1137–1143. [https://doi.org/10.1016/s0021-9258\(19\)75761-5](https://doi.org/10.1016/s0021-9258(19)75761-5).
- 775 [68] P. Beckerson, M.T. Wilson, D.A. Svistunenko, B.J. Reeder, Cytoglobin ligand binding
776 regulated by changing haem-co-ordination in response to intramolecular disulfide bond
777 formation and lipid interaction, *Biochem. J.* 465 (2015) 127–137.

778
779
780
781
782

<https://doi.org/10.1042/BJ20140827>.

- [69] A. Diuba, Data and scripts for “Individual heme a and heme a3 contributions to the Soret absorption spectrum of the reduced bovine cytochrome c oxidase,” 2 (2022).
<https://doi.org/10.17632/DMRKN9PFRR.3>.